International Journal of Petroleum and Petrochemical Engineering (IJPPE)
Volume 8, Issue 1, 2023, PP 18-35
ISSN 2454-7980 (Online)
DOI: http://dx.doi.org/10.20431/2454-7980.0801003
www.arcjournals.org

Closing Thoughts on the Proposition of Improving Drift Velocity Closure Relationship for Multiphase Flow Models

Aniefiok Livinus

Chemical and Petroleum Engineering Department, University of Uyo, P.M.B 1017, Uyo, Akwa Ibom State, Nigeria

Corresponding Author:** ***Aniefiok Livinus, *Chemical and Petroleum Engineering Department, University of Uyo, P.M.B 1017, Uyo, Akwa Ibom State, Nigeria*

Abstract: *The accurate prediction of drift velocity is essential in the modelling of multiphase flow in pipelines. Efforts on enhancing the applicability and predictive capabilities of drift velocity closure relationship in multiphase flow models for both low and high viscous fluids are increasing to better design and manage equipment for the production and transportation of oil resources. This work therefore present recent efforts on the developments of drift velocity models using different approaches, including Artificial Neural Network. The predictive capabilities of the developed models were evaluated by comparing with results from experimental data and existing correlations by error analysis. The outcomes demonstrate that, in overall, the difference in predictions between the developed empirical models and the ANN model is insignificant. However, both models, in most cases, outperform some of the notable drift velocity models available in open literature.*

Keywords: *Rise velocity; Artificial Neural Network; machine learning; multiphase flow modelling; drift flux model.*

Nomenclature

C_o	Constant (in translational velocity)	
D	Pipe diameter	m
Eo	Eötvös Number	
Fr	Froude Number	
Fr_θ	Froude Number at pipe inclination	
g	Acceleration due to gravity	m/s^2
Mo	Morton number	
Re	Reynolds number	
N_{vis}	Viscosity number	
v_d	Drift velocity	m/s
v_d^h	Drift velocity for horizontal flow	m/s
v_d^v	Drift velocity for vertical flow	m/s
v_m	Mixture velocity	m/s
v_t	Translational velocity	m/s
ρ	Density	kg/m^3
μ	Viscosity	$kgm^{-1}s^{-1}$
σ	Surface tension	N/m
θ	Pipe inclination to horizontal	Degree
R	Buoyancy Reynolds number	
Lp	Ratio of surface tension and pipe diameter against liquid density and viscosity (Livinus parameter)	

1. INTRODUCTION

Two phase flow is of high interest in chemical and petroleum industries, and multiphase pipe flow models are essential for a better understanding of the phenomena and to design equipment for the production and transportation of oil resources. Several of these models, for example slug flow models, apply a number of closure relations to link the gas and liquid phases in a one-dimensional two-fluid model approach, see Taitel and Barnea [1], Fabre and Line [2], and Bendiksen [3], for thorough studies on the modelling of two-phase slug flow. The translational velocity, which basically relies on the drift velocity, as shown in Equation (1) proposed by Nicklin [4], is one of such closure relationships in a slug flow model.

$$v_t = C_o v_m + v_d \tag{1}$$

where C_o is approximately 1.2 for turbulent flows and 2.0 for laminar flows, v_m is the mixture velocity (the sum of the superficial liquid and gas velocities), and v_d is the drift velocity – the velocity of the long gas bubble in a stagnant liquid in tube.

As gas bubbles' dynamics are influenced by viscous, inertial, gravitational, and interfacial forces acting on them(White and Beardmore[5]), dimensional analysis has shown that four dimensionless pi -groups are sufficient to determine the bubble dynamics: the Froude number, which is the ratio of the bubble inertia to the gravitational forces; the Eötvös number, which is the ratio of the gravitational to interfacial forces; the Morton number, which at times is seen as the property number; and the inclination angle, measured from the horizontal. The choice of the pi- groups is not unique; for example, the inverse viscosity number, a combination of Eötvös number and Morton number, can also be employed. Several researchers, e.g White and Beardmore[5], Zukoski [6], Weber et al. [7], Carew et al. [8], Viana et al. [9], Gokcal et al. [10]; Jeyachandra et al. [11]; Moreiras et al. [12], Lizarraga-Garcia et al. [13], Livinus et al. [14], and Tang et al. [15], have used different combinations of the dimensionless pi-groups and other set of independent dimensionless groups (Reynolds number, Weber number and buoyancy Reynolds number) to represent the dynamics, especially the drift velocity, of the bubbles found in a two-phase flow. Note that the mathematical definitions of these dimensionless groups can be found in the appendix section of this work.

Table A-1 summarises some of the bubble velocity correlations without the void fraction parameter, available from the open literature. Performance evaluations of several of these models may be found in different past studies, for instance from Viana et al.[9], Jeyachandra et al. [11], Moreiras et al. [12], Lizarraga-Garcia et al. [13], and Livinus et al. [14]. Performance assessments of some drift velocity correlations with void fraction parameter can be found in Bhagwat and Ghajar[16].

Zuber and Findlay [17] confirmed the drift flux relationship provided in Equation (1) for vertical annular and slug flows. Franca and Lahey [18], using air–water experimental data, verified the use of the drift flux model for all flow patterns observed in horizontal gas–liquid flow. Danielson and Fan [19] showed that this relationship is valid for stratified, annular, slug and dispersed bubble flows in a large diameter, horizontal and high-pressure system. In order to extend the drift flux model to a high viscosity liquid, Choi et al. [20, 21] proposed the expression given in Equation (14) with fixed coefficients obtained from a regression analysis between the predicted liquid holdup and the measured liquid holdup. They validated their model, and found fair agreement against the experimental data of Gokcal[22, 10] that include various flow patterns such as stratified wavy, elongated bubble, slug, and annular flow. Unfortunately, proposing such fixed coefficients might affect the predictive strength of a generalised drift velocity model. Bhagwat and Ghajar[16]then proposed a more complex drift flux model applicable over a wide range of flow conditions (holdups and pipe inclinations for both downward and upward flows). Their drift velocity correlation was formulated as a function of pipe orientation, pipe diameter, fluid properties and void fraction. However, Tang et al. [15] reported numerous discontinuities embedded within the Bhagwat and Ghajar[16] model, thus making it ineligible for implementation in a fully coupled numerical system. Tang et al. [15]also formulated a drift velocity equation as a function of pipe orientation, pipe diameter, fluid properties and void fraction, with dimensionless "viscosity" number and Eötvös number. They reported that the horizontal section of their drift velocity equation was partly inspired by the work of Zukoski [6], Ben-Mansour et al. [23], and Jeyachandra et al. [11], and was the outcome of various in-house studies conducted by Schlumberger, which was confidential. Hence, detailed information regarding the exact derivation was missing in their publication.

This work therefore offers concise information on the developments of drift velocity models based on different approaches, including Artificial Neural Network. Firstly, the modified version of the Livinus et al.[14] generalised drift velocity correlation was considered, see Livinus [24], and Livinus and Verdin[25]. The predictive capabilities of the developed models were evaluated by comparing with results from experimental data and existing correlations by error analysis.

2. MODIFIED VERSION OF THE LIVINUS ET AL.[14] MODEL

Livinus et al.[14] pointed out that most of the non-complex existing drift velocity models have shown wide applicability limitations, and sometimes low predictive capabilities, either because they were derived from data with a narrow range of experimental parameters or because of their formulation. In their bid to address these shortcomings, they proposed a simplified generalised drift velocity correlation of the power law form. Calculation errors were however associated with the expressions given in their work, labelled hereafter Equations (A-17b) and (A-17c).Looking closely at those, Equation(A-17c)seems to suggest the same drift velocity value for both vertical and horizontal flows; this is contrary to existing theoretical and experimental results. The first term in Equation (A-17b) was indeed wrongly represented, therefore resulting in a calculation error whenever the buoyancy Reynolds number was greater than the Eötvös number.

The modified formulation provided through Equations 2(a-f),is based on the fitting of the third-degree polynomial of the Livinus et al. [14] gathered dataset, considering the log-log relationship between the Froude number and a combination of the Eötvös number and the buoyancy Reynolds number. This was considered for matching the vertical and horizontal flow data and for having the least percentage error spread.

$$Fr^{H} = 10^{-m} \tag{2a}$$

$$m = (-0.02861x^{3}) + (0.5987x^{2}) + (-4.139x) + 9.843 \tag{2b}$$

$$Fr^{V} = 10^{-n} \tag{2c}$$

$$n = (-0.01386x^{3}) + (0.267x^{2}) + (-1.727x) + 4.167 \tag{2d}$$

$$x = Log_{10}(REo) \tag{2e}$$

$$Fr^{\theta} = Fr^{H}cos\theta + Fr^{V}sin\theta \tag{2f}$$

Other curve fitting models evaluated include the power law model of the form, $y = a * x^{b} + c$, and the exponential law model with two terms of the form, $y = a * \exp(b * x) + c * \exp(d * x)$. The curve fitting parameters for these two models and their R-squared values are presented in Tables1 and 2, respectively.

Table1. *Variables for the two-term power law model($y = a * x^{b} + c$)*

Data	*a*	*b*	*c*	R^2
0-2-degree	1044	-5.378	0.3433	0.905
0 – 90-degree	-16.38	0.06146	18.63	0.797
90-degree	-5.099	0.1927	7.568	0.8625

Table2. *Variables for the two-term exponential law model($y = a * exp(b * x) + c * exp(d * x)$)*

Data	*a*	*b*	*c*	*d*	R^2
0-2-degree	3.355E+04	-3	1.429	-0.1989	0.9137
0 – 90-degree	4.484	-0.4922	0.01886	0.3109	0.8738
90-degree	4.571	-0.4934	0.01619	0.3989	0.9373

It is worth mentioning that there were no significant differences among the three major tested curve fitting models. The two-term exponential model happens to predict more of the gathered drift velocity data in the ±20% error bandwidth, as shown in the probability density function (PDF) plot in Figure 1(a). However, the three-degree polynomial curve fitting model displays the least error spread. Figure 1(b) shows the count of the number of the gathered data set with percentage error predictions between -100% and 1000%; it is about 10% of the gathered data set for the two-term exponential model, 4% for the power law model and about 1% for the three-degree polynomial model.

It should also be noted that poor predictions were obtained with the two-term exponential model for fluid flow conditions with both the buoyancy Reynolds numbers and the Eötvös numbers higher than 200.

The modified Livinus et al.[14]drift velocity correlation was evaluated and found to agree well, as shown in Figure 2,for fluid conditions in a wide range of viscosity, (0.544cP ~ 7120cP), and for upwardly inclined pipes between 0° and 90°. However, for very high viscous liquid flowing in a pipe and fluid conditions where both the Eötvös numbers and the buoyancy Reynolds numbers are less than 200, the generalised model did not perform well, as may be seen in Figure 2(b).

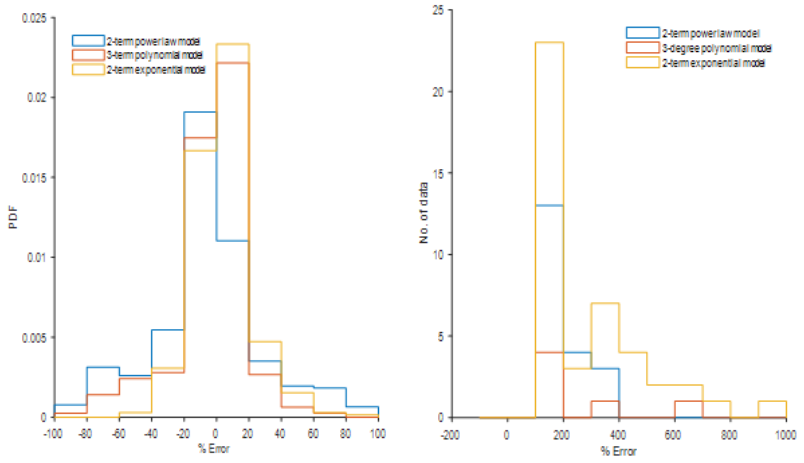

(a) *PDF % error plot among the three tested models* (b) *No. of data count plot among the three tested models*

Figure1. *Performance comparisons for the three tested curve fitting models*

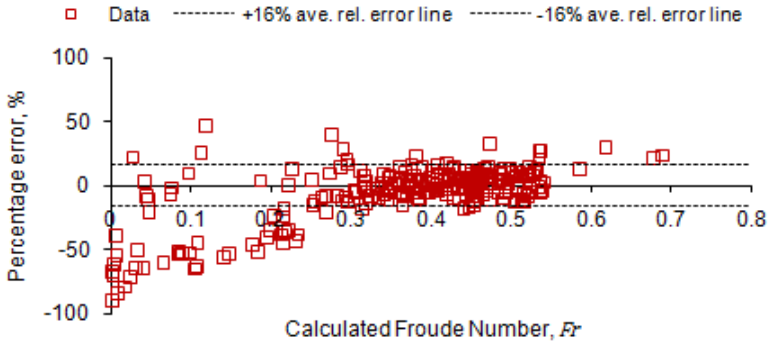

(a) Percentage error vs calculated Froude number

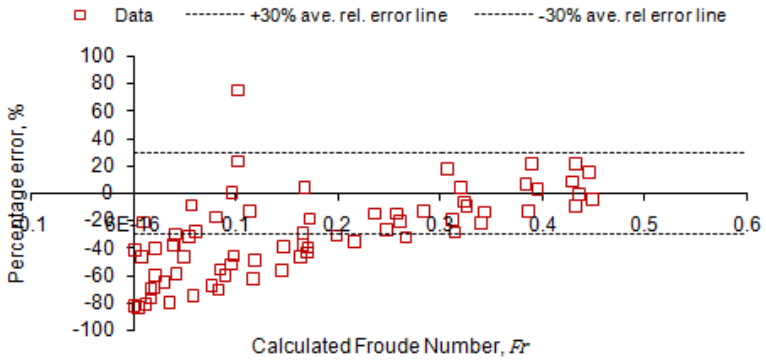

(b) Percentage error vs calculated Froude number for pipe and fluid conditions where both the Eötvös numbers and the buoyancy Reynolds numbers are less than 200

Figure2. *Performance of the new drift velocity correlation on the gathered experimental dataset*

Based on the above graphs, the need for developing and testing other methods for improving the drift velocity model formulation became apparent. A series of drift velocity correlations, especially for pipe and fluid conditions for both the Eötvös numbers and the buoyancy Reynolds numbers being less than 200was then considered. The application of Artificial Neural Network was also investigated for the drift velocity model formulation, in a bid to develop an improved generalised model.

3. DEVELOPMENT OF DRIFT VELOCITY CORRELATIONS FOR EÖTVÖS AND BUOYANCY REYNOLDS NUMBERS LESS THAN 200

The reported dataset from Livinus et al.[14] was used in this study. Having critically analysed this dataset, it appears that the Froude numbers display different curve patterns: a typical curve increases from zero-degree (horizontal flow), reaches a wide maximum for angles of inclination between 30°and 60°, and then decreases to 90° (vertical flow). This is more apparent as the Froude number increases. Keeping in mind the different curve patterns and the gathered data, a parameter able to describe those curve patterns can be defined as the ratio of the pipe diameter and the surface tension to the liquid viscosity and its density, hereafter denoted 'Livinus parameter', Lp.

$$Lp = \frac{\sigma D}{\rho_l \mu} \tag{3}$$

Figure 3 shows the gathered data for the different curve patterns under various range of the Livinus parameter Lp. AsLpdecreases, Fr also decreases, this is largely due to the influence of the fluid viscosity and pipe diameter.

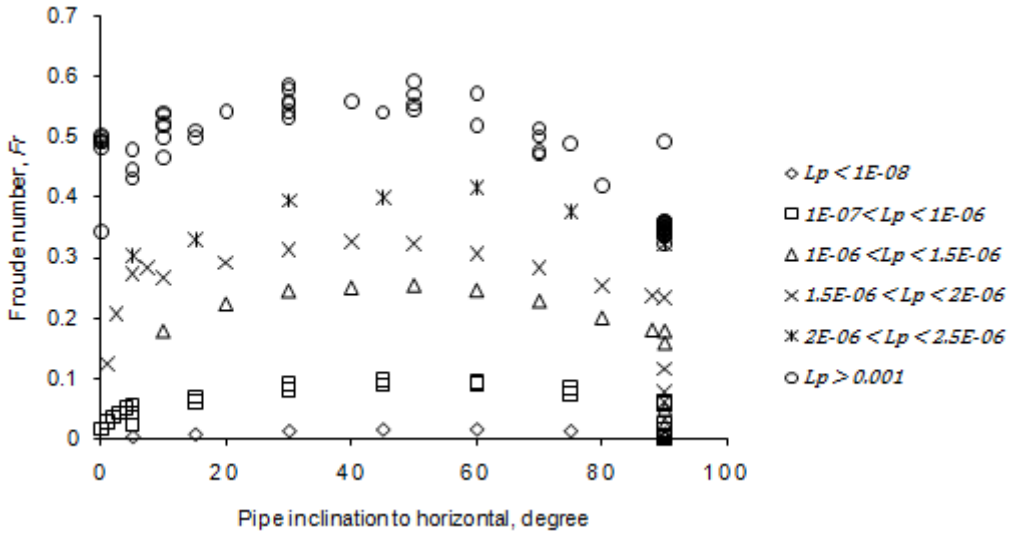

Figure3. *Froude number vs Pipe inclination at various Lp*

The resulting series of drift velocity correlations could be formulated, based on the fitting of the trigonometric relationship of the Froude numbers under the various Lp values.A general form could be established as:

$$Fr^{\theta} = Acos(B\theta) + Csin(B\theta) \tag{4}$$

Constants A, B and C for the various Lp valueswith sufficient gathered data for fitting, are provided in Table 2, for pipe and fluid conditions where the Eötvös and buoyancy Reynolds numbers are less than 200.The R-squared values range from 0.67 to 0.99. Figure 4 shows the curve fittings for the first fourLpcases listed in Table 3.

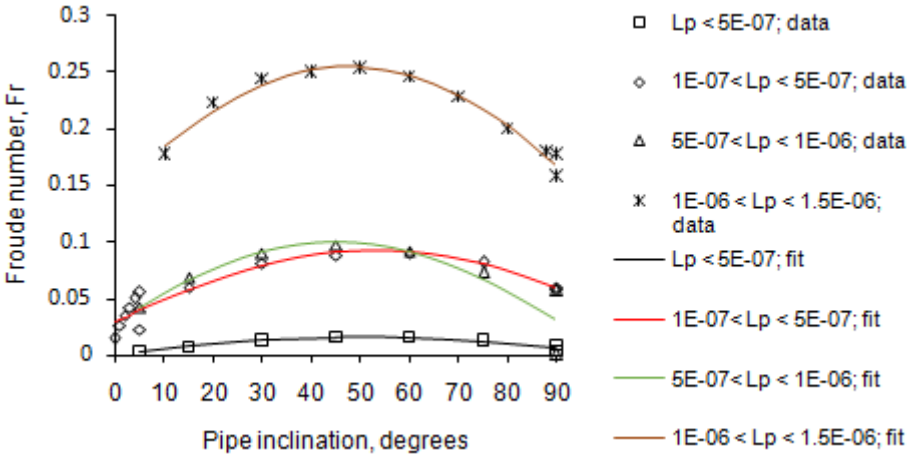

Figure4. *Curve fitting for the first four Lp cases*

Table3. *Fitting constants; A, B and C for various Lp*

Lp	*A*	*B*	*C*
Lp< 1.00E-07	1.04E-04	1.76E+00	1.63E-02
1.00E-07<*Lp*<5.00E-07	2.93E-02	1.36E+00	8.81E-02
5.00E-07<*Lp*< 1.00E-06	2.92E-02	1.61E+00	9.58E-02
1.00E-06 <*Lp*< 1.50E-06	1.46E-01	1.16E+00	2.09E-01
1.50E-06 <*Lp*< 2.00E-06	1.96E-01	1.26E+00	2.74E-01
2.00E-06 <*Lp*< 2.50E-06	2.72E-01	9.67E-01	3.10E-01
2.50E-06 <*Lp*< 2.70E-06	1.39E-03	1.55E+00	2.13E-01
2.70E-06 <*Lp*< 3.00E-06	2.51E-01	9.45E-01	2.49E-01
4.00E-06 <*Lp*< 4.25E-06	2.97E-01	9.34E-01	2.51E-01
4.25E-06 <*Lp*< 4.50E-06	3.22E-01	8.96E-01	2.42E-01
4.50E-06 <*Lp*< 6.00E-06	2.60E-01	1.10E+00	3.43E-01
6.00E-06 <*Lp*< 7.00E-06	3.30E-01	9.42E-01	2.80E-01
7.00E-06 <*Lp*< 8.00E-06	2.82E-01	1.07E+00	3.46E-01
8.00E-06 <*Lp*< 9.00E-06	3.29E-01	9.75E-01	3.03E-01
9.00E-06 <*Lp*< 1.00E-05	3.44E-01	9.81E-01	3.05E-01
1.40E-06 <*Lp*< 1.50E-05	1.11E-01	1.32E+00	3.46E-01

4. APPLICATION OF ARTIFICIAL NEURAL NETWORK (ANN) TO MODEL THE DRIFT VELOCITY

As pointed out by Brunton et al.[26], extensive efforts are needed to gain insights and mechanistic understanding, through analysis of observations and data from experiments, to develop closure models that effectively represent data in a compact form. These may be seen in the formulations of the modified Livinus et al.[14] models and the developed series of drift velocity correlations under various Livinus parameters. As an alternative to mechanistic and semi-analytical models, machine learning (ML) methodologies become attractive as they can be used to capture any underlying data correlation using nonparametric models, or so-called data-driven models. In the past three decades, Neural Networks have become of interest to fluid engineers, and supervised training algorithms, specifically back propagation algorithm, have been commonly applied (Amini and Mohaghegh, [27]).Recently, Nathaniel and Livinus [28] developed an ANN drift velocity model for all pipe inclination; the predictions were found to agree well with experimental data, for fluid conditions in a wide range of viscosity, and for upwardly inclined pipes between 0° and 90°. Koffi and Livinus [29] applied deep learning approach to model the drift velocity. Unfortunately, for very high viscous liquid flowing in a pipe and fluid conditions where both the Eötvös and buoyancy Reynolds numbers were less than 200, the model also did not perform well. For this reason, we have therefore attempted to apply the ANN to develop models for vertical flow, horizontal flow and inclined flow, separately.

The basic idea of Artificial Neural Network is to approximate a function, f^*, between input vector, x, to output category, y, that is:

$$\hat{y} = f^*(x) \tag{5}$$

The mapping between input and output is given by;

$$\hat{y} = f^*(x, \theta) \tag{6}$$

where, θ consists of weight, w, and bias, b. θ is learnt by iterating over a given data.

An Artificial Neural Network comprises at least three layers: input layer, hidden layer with neurons, and output layer. Each layer connects with other layers with the help of weights. The network performance is solely based on the adjustment of weights between these layers. Hidden layers assigned with transfer function are usually 'log-sigmoidal' or 'tan-sigmoidal'. Output layer is assigned with 'pure linear' activation function (Elkatatny and Mahmoud, [30]). The above explanation is expressed mathematically as;

$$\hat{y} = \sigma(x^T w + b) \tag{7}$$

where, σ is the transfer function, usually log-sigmoidal or tan-sigmoidal, and x^T is the transpose of the input vector, x.

Detailed information regarding the development of drift velocity models using Artificial Neural Networks for vertical, inclined and horizontal pipes is provided in the following. Once again, the dataset from Livinus et al.[14] was used. Pipe and fluid parameters used to develop the models are given in Table 4.These data were normalized using Equation 8 for the various pipe orientations.

$$X_n = \frac{X - X_{min}}{X - X_{max}} \tag{8}$$

were X_n is the normalized value,X isthe original value, X_{min} is the minimum of the original values, and X_{max} is the maximum of the original values.

Table4. *Statistical analyses of the pipe and fluid parameters*

Pipe orientation	Range of values	Pipe ID (m)	Liquid density Kg/m^3	Liquid viscosity cP	Surface tension N/m	Froude number
Horizontal	**Min**	2.20E-02	8.60E+02	1.00E+00	1.51E-02	1.49E-02
	Max	1.52E-01	9.98E+02	1.14E+03	7.20E-02	5.05E-01
	Average	7.03E-02	9.02E+02	2.73E+02	3.42E-02	3.24E-01
Vertical	**Min**	4.00E-03	7.87E+02	5.44E-01	2.02E-02	5.90E-05
	Max	1.52E-01	1.51E+03	3.33E+04	8.70E-02	3.88E-01
	Average	4.15E-02	1.04E+03	1.19E+03	4.57E-02	2.31E-01
Inclined	**Min**	4.00E-03	7.87E+02	5.44E-01	2.02E-02	5.90E-05
	Max	1.52E-01	1.51E+03	3.33E+04	8.70E-02	3.88E-01
	Average	4.15E-02	1.04E+03	1.19E+03	4.57E-02	2.31E-01

The MATLAB® Neural Network tool was used for the development of the drift velocity neural network models. The models for the horizontal and vertical pipes were developed using four input parameters: pipe ID, liquid density, liquid viscosity and surface tension. However, for inclined pipes, one additional input parameter was considered, the pipe inclination value. The Feed-Forward network was used with the Back Propagation algorithm. The network was trained using the Bayesian Regularization (BR) algorithm because of its ability to give good generalization for difficult, small or noisy datasets. Other algorithms have been tested, the Levenberg-Marquardt (LM) and the Scaled Conjugate Gradient (SCG), but the Bayesian Regularization algorithm provided the best results.

The number of neurons to be used in the hidden layer had to be established. The most common approach for determining this value is through trial-and-error. Three to seven neurons were tested, the three-neuron case generated the best results, and was thus considered to develop the models. Note that for the inclined cases, the five-neuron procedure worked better.Figure 5 shows the network architecture.

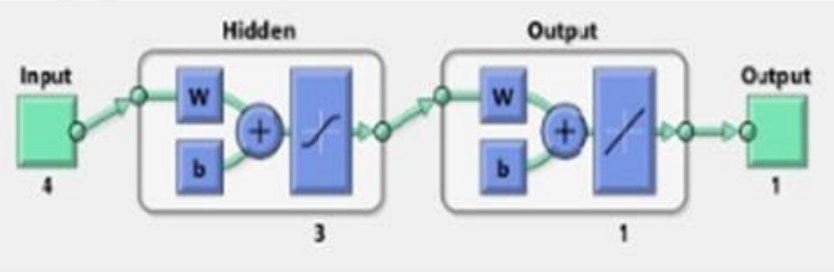

Figure5. *Neural Network Architecture*

Based on a70:5:25 partition, 70%of the data was used for training, 5% for validation and 25% for testing. Such partition was applied as the Bayesian Regularization only makes use of the training and testing data, ignoring the validation phase (the lowest percentage here) in order to avoid over fitting.

4.1. Results of the Artificial Neural Networks for the Drift Velocity in Horizontal Pipes

The normalized expressions for the data used for the development of the Neural Network model for horizontal pipes are given fromEquations9to 13:

$$(ID_p)_n = 7.669ID_p - 0.169 \quad (9)$$

$$(\gamma_l)_n = 0.007\gamma_l - 6.232 \quad (10)$$

$$(\mu_l)_n = 0.001\mu_l - 0.001 \quad (11)$$

$$(T_s)_n = 17.575T_s - 0.265 \quad (12)$$

$$(N_F)_n = 2.042N_F - 0.03 \quad (13)$$

where$(ID_p)_n$, $(\gamma_l)_n$, $(\mu_l)_n$, $(T_s)_n$and $(N_F)_n$are the normalized values of Pipe ID, liquid density, liquid viscosity, surface tension, and Froude number, respectively.

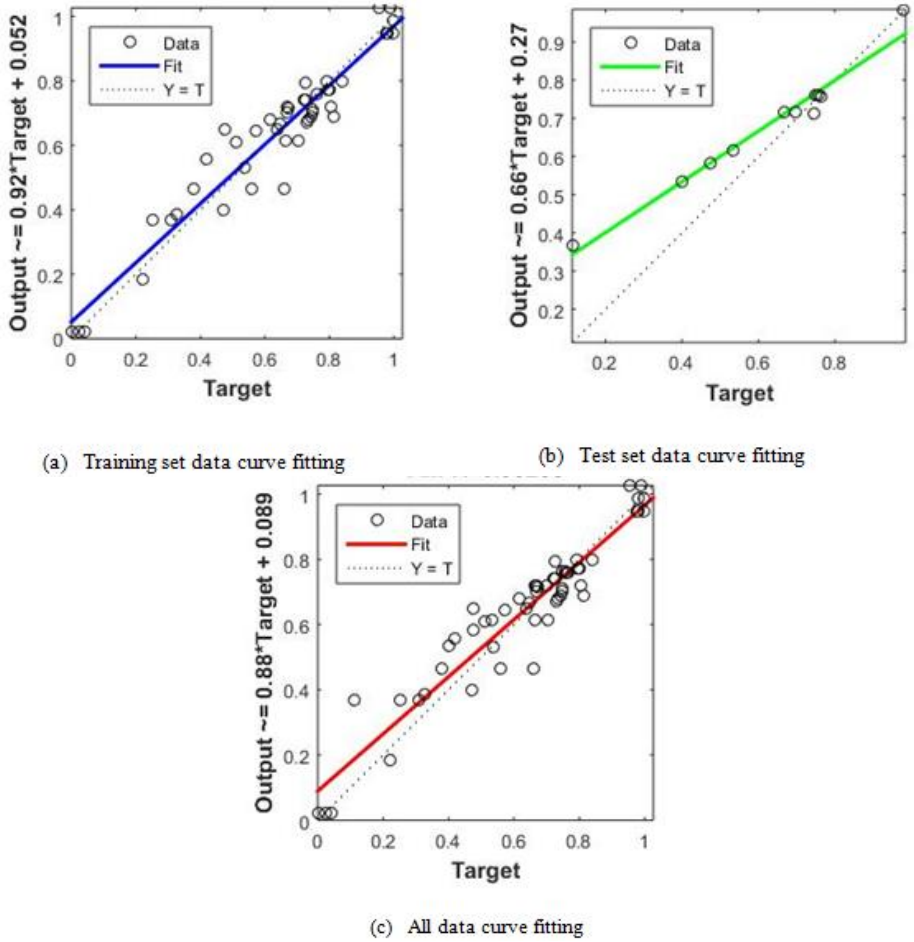

(a) Training set data curve fitting

(b) Test set data curve fitting

(c) All data curve fitting

Figure6. *Network regression plots for horizontal flow*

Figure 6 shows the regression plots for the training and testing performance, as well as the overall performance of the developed model. The target in the plots represent the experimental Froude numbers, while the output denotes the predicted Froude numbers. With R-squared values of 0.96, 0.98 and 0.95 for the training, testing and overall performance respectively, the model appears to perform well for predicting the observed Froude number in horizontal pipes.

4.1.1. Artificial Neural Network Equation – Horizontal Pipe

The weights (w) and biases (b) of the Neural Network model were utilized to derive the normalized value of the Froude number:

$$(N_F)_n = \sum_{i=1}^{3} w2_i(w1_{i,1}(ID_p)_n + w1_{i,2}(\gamma_l)_n + w1_{i,3}(\mu_l)_n + w1_{i,4}(T_s)_n + b1_i) + b2 \quad (14)$$

where i denotes the index of each neuron in the hidden layer, $w1_i$ is the weight associated with input and hidden layers for each input parameter, $b1_i$ denotes the biases associated with the input and training layers, $w2_i$ is the weight associated with the hidden and output layers, and $b2$ is the bias associated with the hidden and output layers. All weights and biases considered here are summarized in Table 5.

Table5. *Weights and Biases of the developed Neural Network – horizontal pipe*

Neuron index	$(\boldsymbol{w1})$				$(\boldsymbol{w2})$	$(\boldsymbol{b1})$	$(\boldsymbol{b2})$
	$(\boldsymbol{ID_p})_n$	$(\boldsymbol{\gamma_l})_n$	$(\boldsymbol{\mu_l})_n$	$(\boldsymbol{T_s})_n$			
1	0.3699	-0.0862	-0.0251	0.1142	-0.3607	-0.0266	-0.2307
2	0.2038	-0.4180	0.2792	-0.1698	-0.5205	-0.1580	
3	-1.4818	0.2063	0.6478	-0.3029	-0.9897	-0.8412	

4.2. Results of the Artificial Neural Networks for the Drift Velocity in Vertical Pipes

The normalized expressions for the data used for the development of the Neural Network model for vertical pipes are given by Equations15 through 19:

$$(ID_p)_n == 6.739ID_p - 0.027 \quad (15)$$

$$(\gamma_l)_n = 0.001\gamma_l - 1.089 \quad (16)$$

$$(\mu_l)_n = 0.00003\mu_l - 0.00002 \quad (17)$$

$$(T_s)_n = 14.97T_s - 0.302 \quad (18)$$

$$(N_F)_n = 2.580N_F \quad (19)$$

Similarly, to horizontal pipes, the regression plot for the training and testing performance were plotted, along with the overall performance of the developed model, as can be seen in Figure 7. R-squared values of 0.96, 0.95 and 0.96 for the training, testing and overall performance were obtained. This demonstrates that the developed model performs well for predicting experimental-based Froude numbers in vertical pipes.

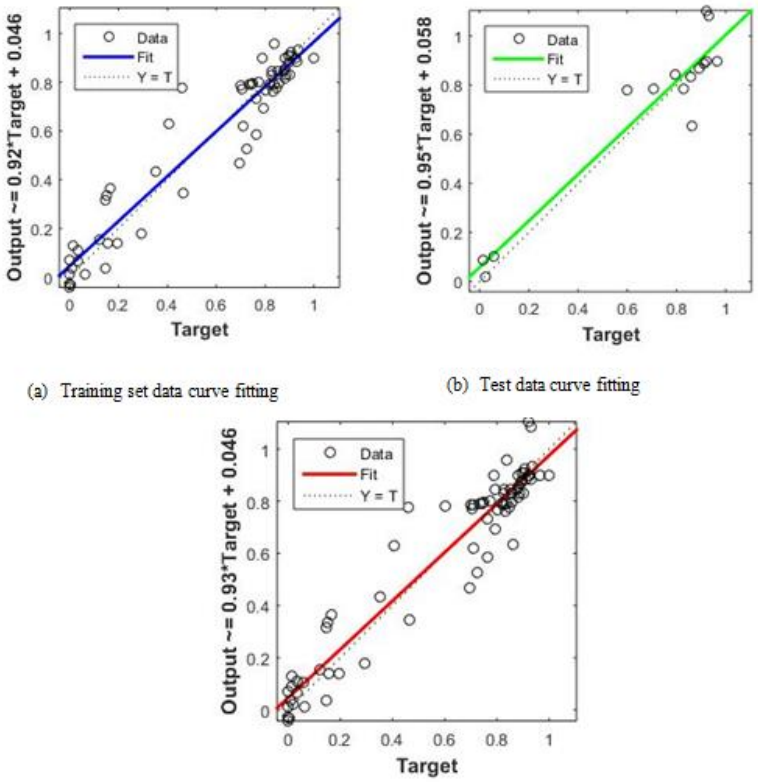

Figure7. *Network regression plots for vertical flow*

4.2.1. Artificial Neural Network Equation – Vertical Pipe

An equation was extracted from the optimized ANN results to derive the normalized value of the Froude number for vertical pipes, and all corresponding weights and biases are summarised in Table 6

$$(N_F)_n = \sum_{i=1}^{3} w2_i(w1_{i,1}(ID_p)_n + w1_{i,2}(\gamma_l)_n + w1_{i,3}(\mu_l)_n + w1_{i,4}(T_s)_n + b1_i) + b2 \quad (20)$$

Table6. *Weights and Biases of the developed Neural Network – vertical pipe*

Neuron index	$(\boldsymbol{w1})$				$(\boldsymbol{w2})$	$(\boldsymbol{b1})$	$(\boldsymbol{b2})$
	$(\boldsymbol{ID_p})_n$	$(\boldsymbol{\gamma_l})_n$	$(\boldsymbol{\mu_l})_n$	$(\boldsymbol{T_s})_n$			
1	0.0538	2.9201	-1.0710	1.7872	1.8778	0.3777	0.0347
2	-0.0854	0.0469	-0.2582	2.0988	-1.9735	0.4510	
3	-2.6605	1.8051	3.3345	-1.1284	-1.0921	1.1931	

4.3. Results of the Artificial Neural Networks for Drift Velocity Development for Inclined Pipes

The normalized expressions for the data used for the development of the Neural Network model for inclined pipes are given by Equations21 through 26:

$$(ID_p)_n = 6.739ID_p - 0.027 \quad (21)$$

$$(\gamma_l)_n = 0.001\gamma_l - 1.089 \quad (22)$$

$$(\mu_l)_n = 0.00003\mu_l - 0.00002 \quad (23)$$

$$(T_s)_n = 13.908T_s - 0.21 \quad (24)$$

$$(N_F)_n = 1.683N_F \quad (25)$$

$$(\theta_p)_n = 0.011\theta_p \quad (26)$$

with all expressions as defined previously, and $(\theta_p)_n$ the normalized value of pipe inclination (angle).

Figure 8 shows the regression plot for the training and testing performance, as well as the overall performance of the developed model. R-squared values of 0.97, 0.96 and 0.97 were obtained for the training, testing and overall performance, respectively. Once again, the approach worked well here for inclined pipelines.

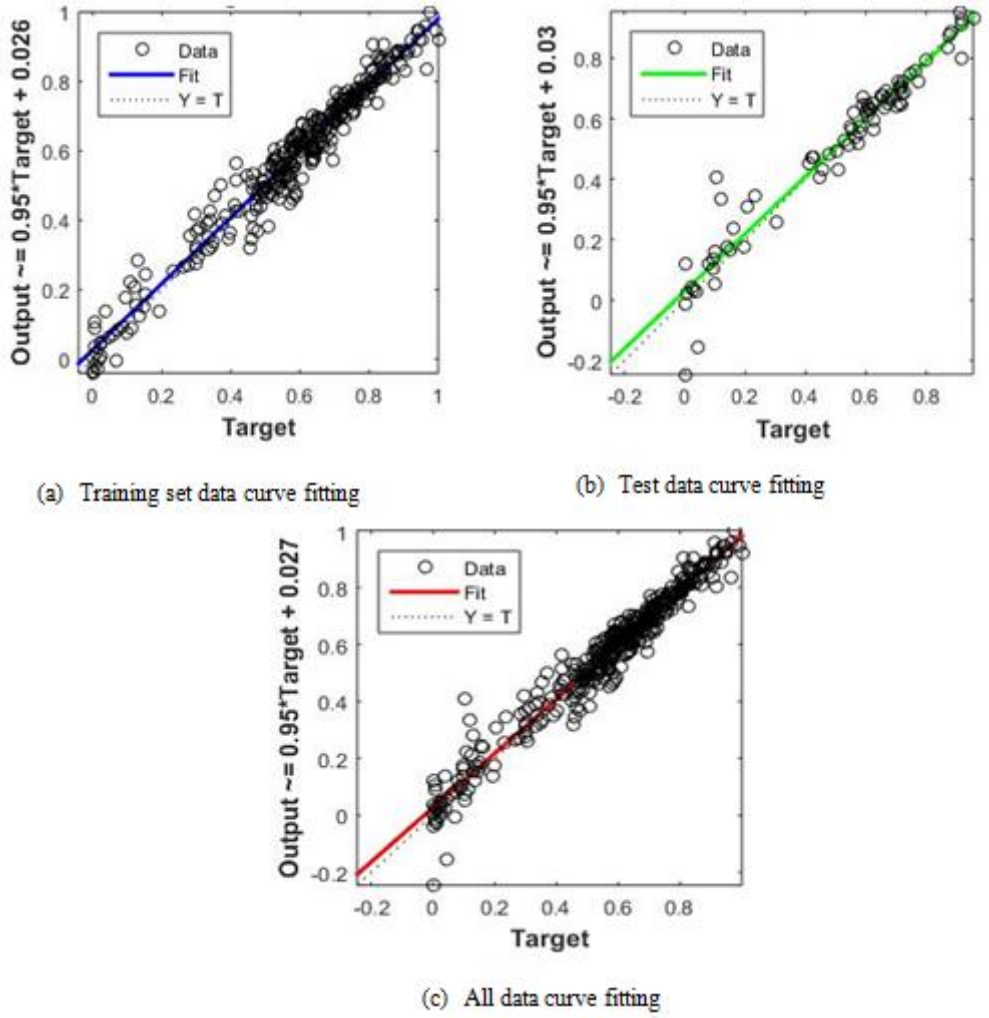

Figure8. *Network regression plots for inclined flow*

4.3.1. Artificial Neural Network Equation – Inclined Pipe

Finally, an equation was extracted from the optimized ANN results to derive the normalized value of the Froude number for inclined pipes. All corresponding weights and biases are summarised in Table 7. As explained previously, a five-neurons procedure was best in the hidden layer when dealing with inclined pipes.

$$(N_F)_n = \sum_{i=1}^{5} w2_i(w1_{i,1}(ID_p)_n + w1_{i,2}(\theta_p)_n + w1_{i,3}(\gamma_l)_n + w1_{i,4}(\mu_l)_n + w1_{i,5}(T_s)_n + b1_i) + b2 \quad (27)$$

Table7. *Weights and Biases of the developed Neural Network – inclined pipe*

Neuron index	$(\boldsymbol{w1})$					$(\boldsymbol{w2})$	$(\boldsymbol{b1})$	$(\boldsymbol{b2})$
	$(\boldsymbol{ID_p})_n$	$(\boldsymbol{\theta_p})_n$	$(\boldsymbol{\gamma_l})_n$	$(\boldsymbol{\mu_l})_n$	$(\boldsymbol{T_s})_n$			
1	-0.1632	-0.1071	1.8405	8.5645	-1.2901	-1.7602	8.8275	-4.6168
2	0.1493	-0.5997	-0.4591	-0.3565	0.1325	-2.2819	-1.2886	
3	-0.2708	0.3155	-5.4054	0.1941	2.3336	-0.6975	-0.3333	
4	-0.0147	-0.2625	0.2398	1.5162	-0.1782	5.3907	1.9822	
5	1.2383	0.3687	-0.6858	-2.9856	-0.0468	2.1767	-1.4281	

5. COMPARATIVE ANALYSES OF THE PERFORMANCES OF SEVERAL DRIFT VELOCITY CORRELATIONS AGAINST THE NEWLY DEVELOPED MODELS

The performance of the novel models, the modified Livinus et al.[14] model, the series of drift velocity correlations with Eötvös and buoyancy Reynolds numbers lower than 200, and the ANN models, were compared with the performances of some of the correlations listed in Table A-1, in their respective ranges of validity. As may be seen from the probability density function of the percentage error plots in Figures9 to 11, the modified Livinus et al and the ANN models, overall performed better than the other correlations under their respective range of validity.

For the vertical flow models assessment, the modified Livinus et al. and the ANN models performed significantly better than the Wallis [31] model, see Figure 9(a). Looking at Figure 9(b), the Tung and Parlange [32] model appears to have better-matched results than the three-degree polynomial model from Livinus et al. and the ANN model. However, when looking closely, the overall performance of both the three-degree polynomial and the ANN models are actually similar to that of the Tung and Parlange[32] model as all three models have over 85% of the predicted data within the ±20% error range.

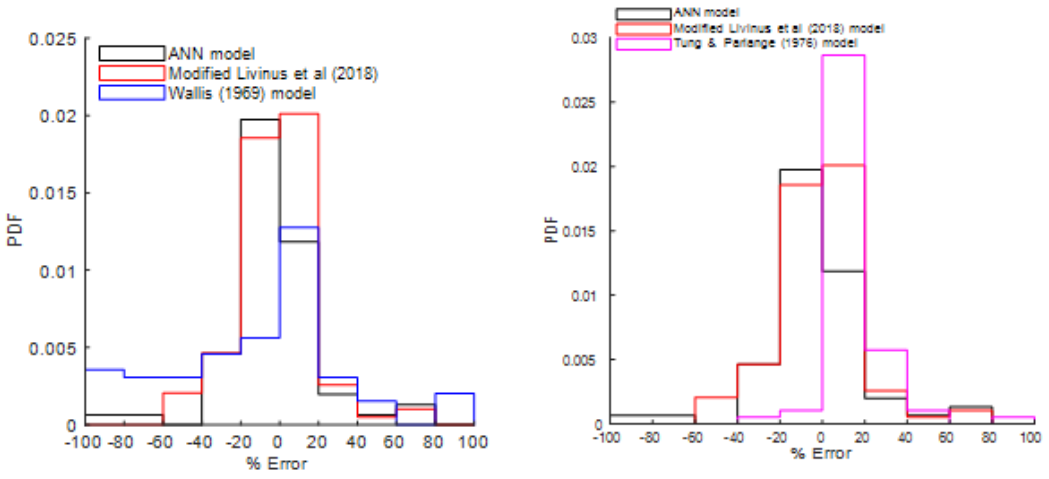

(a) Wallis [31] vs new models (b) Tung and Parlange[32] vs newmodels

Figure9. *Comparison of the new models (Livinus et al. 2018, and ANN), with other models from the literature - vertical pipe flow*

For the horizontal flow models comparisons, the modified Livinus et al. model and the ANN model outperform the Weber [33] model, see Figure 10(a). The recently developed Pablo Valdés et al.[34] model as presented in Equation (A-18) with an exponential term, is an improvement to the horizontal flow model of Moreiras [12];its performance is similar to both the three-degree polynomial and ANN models, see Figure 10(b).

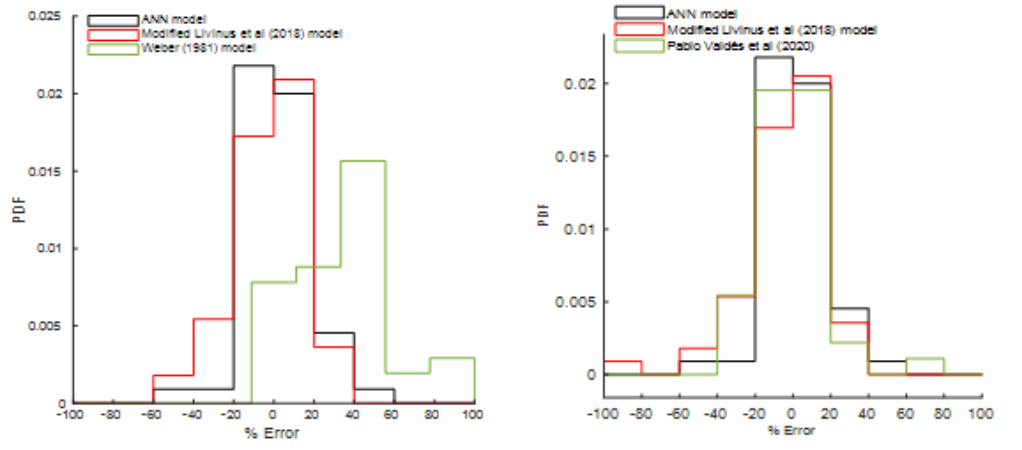

(a) Weber [33] vs new models (b) Pablo Valdés et al.[34] vs new models

Figure10. *Comparison of the new models (Livinus et al. [14], and ANN) with other models - horizontal flow*

For models under their validity range for all pipe inclinations and liquid viscosities, the modified Livinus et al.[14] and the ANN models appeared superior when compared to predicted results with the Weber [7], Jeyachandra et al.[11], and Moreiras [12] models, see Figure 11(a, b, and c). For a liquid viscosity of 1cP and for all pipe inclinations within their range of validity, the ANN model showed the best performance. The Bendiksen [35] model seemed to have a larger set of predicted data within the ±20% error bandwidth compared to the modified Livinus et al.[14]model, see Figure 11(d), but overall the percentage error spread is wider than that of the new models.

For very high viscous liquid flowing in a pipe and fluid conditions where both the Eötvös numbers and the buoyancy Reynolds numbers are less than 200, both the Livinus et al. model and the ANN model poorly predicted the observed Froude numbers, as can be seen in Figure 12.

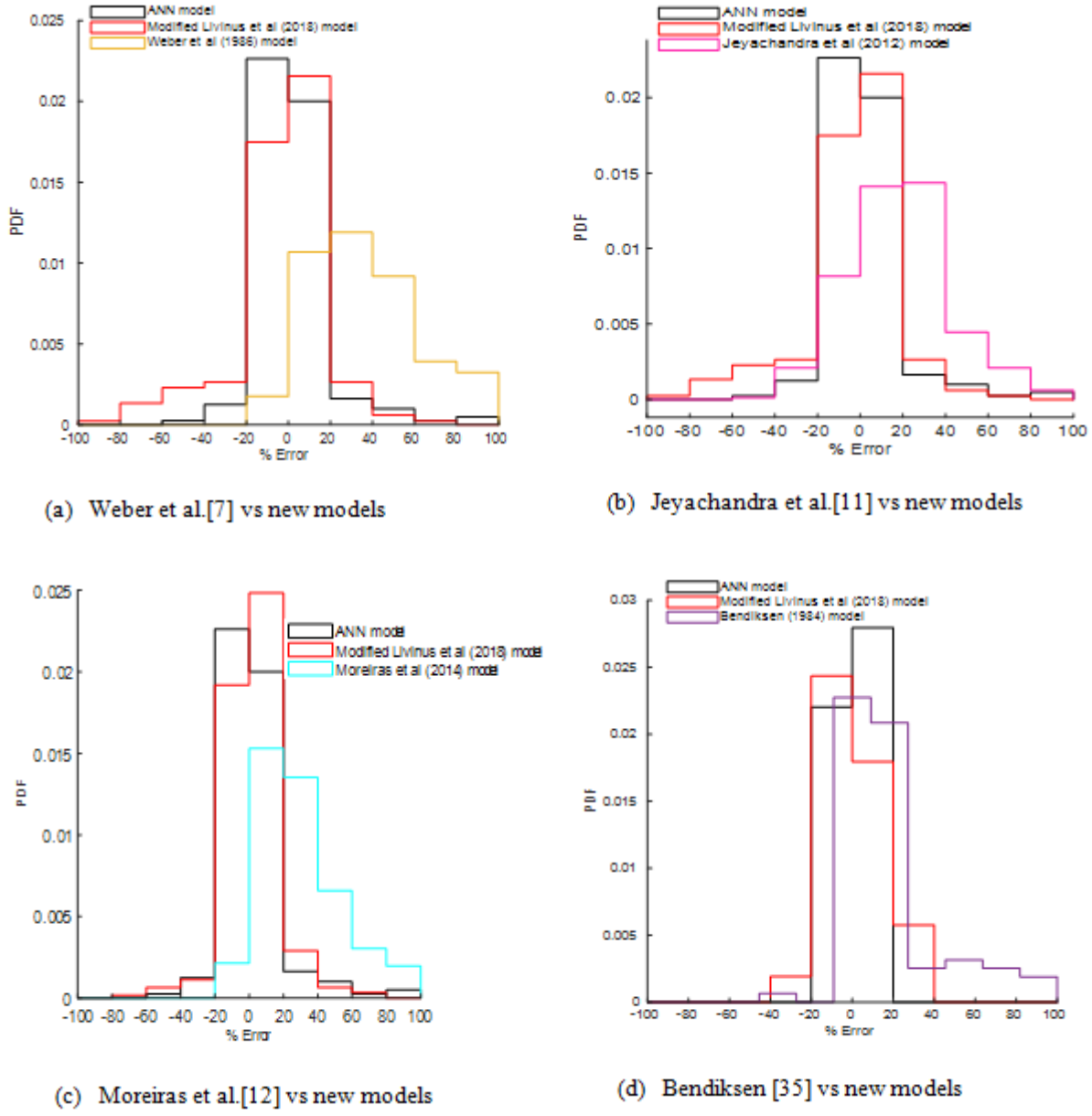

Figure11. *Comparison of the new models (Livinus et al. [14], and ANN)with other models under vertical, horizontal and inclined flows.*

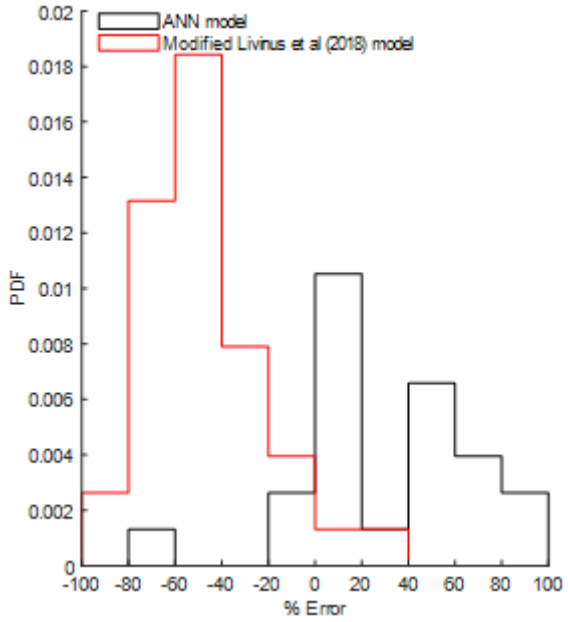

Figure12. *Comparison of the new models (Livinus et al. [14], and ANN) under vertical, horizontal and inclined flows, with Eötvös and buoyancy Reynolds numbers lower than 200*

6. CONCLUSION

Improved drift velocity correlations for the modelling of multiphase flow in pipelines have been presented. The modified Livinus et al. [14] model on drift velocity predictions was presented first. This model is based on the fitting of a third-degree polynomial, considering the log-log relationship between the Froude number and a combination of the Eötvös and buoyancy Reynolds numbers. Predicted results obtained with this newdrift velocity correlation matched well data for fluid conditions within a wide range of viscosity (0.544cP ~ 7120cP), and for upwardly inclined pipes between 0^o and 90^o.

However, for very high viscous liquid, in a pipe and fluid conditions where both the Eötvös and the buoyancy Reynolds numbers are less than 200, the generalised model performed poorly. A series of drift velocity correlations have therefore successfully been developed, based on the fitting of a trigonometric relationship of the Froude numbers under various (Livinus) Lp values.

An ANN approach was also successfully applied for the development of drift velocity models for vertical, horizontal and inclined flows. Comparative analyses of the new developed models, i.e. the modified Livinus et al. [14] and ANN models were performed against other models extracted from the literature and tested under their respective range of validity. It appeared clearly that the modified Livinus et al.[14] model and the series of drift velocity models under various Lp parameters outperformed existing correlations. These new models could therefore improve existing multiphase flow pipeline simulators, and be applied for a better design and improved operations of both viscous and less viscous oil production, processing and transportation.

REFERENCES

[1] Taitel, Y., Barnea, D., (1990) Two-phase slug flow. Adv. Heat Transfer 20, 83–132.

[2] Fabre, J., Liné, A., (1992) Modeling of two-phase slug flow. Annu. Rev. Fluid Mech. 24, 21–46.

[3] Bendiksen, K.H., Malnes, D., Nydal, O.J., (1996) On the modelling of slug flow. Chem. Eng. Commun. 141, 71–102.

[4] Nicklin, D.J., (1962) Two-phase bubble flow. Chemical Engineering Science. 17(9), 693–702.

[5] White, E.T. and Beardmore, R.H., (1962) The velocity of rise of single cylindrical air bubbles through liquids contained in vertical tubes. Chemical Engineering Science. 17(5), pp. 351–361.

[6] Zukoski, E.E., (1966) Influence of viscosity, surface tension, and inclination angle on motion of long bubbles in closed tubes. Journal of Fluid Mechanics. 25(04), 821-837.

[7] Weber, M.E., Alarie, a. and Ryan, M.E., (1986) Velocities of extended bubbles in inclined tubes. Chemical Engineering Science. 41(9), 2235–2240.

[8] Carew, P.S., Thomas, N.H., Johnson, A.B., (1995) A physically based correlation for the effects of power law rheology and inclination on slug bubble rise velocity. Int. J. Multiphase Flow 21, 1091–1106. Printed.

[9] Viana et al., (2003) Universal correlation for the rise velocity of long gas bubbles in round pipes. J. Fluid Mech. 494, 379-398. DOI: 10.1017/S0022112003006165.

[10] Gokcal, B., Al-Sarkhi, a S. and Sarica, C., (2008) Effects of high oil viscosity on drift velocity for upward inclined pipes. SPE Annual Technical Conference and Exhibition, ATCE 2008. September 21, 2008 - September 24, 2008, 2(September), pp. 963–975.

[11] Jeyachandra, B.C., Gokcal, B., Al-Sarkhi, A., Sarica, C. and Sharma, A., (2012) Drift-Velocity Closure Relationships for Slug Two-Phase High-Viscosity Oil Flow in Pipes. SPE Journal.

[12] Moreiras, J., Pereyra, E., Sarica, C. and Torres, C.F., (2014) Unified drift velocity closure relationship for large bubbles rising in stagnant viscous fluids in pipes. Journal of Petroleum Science and Engineering. 124, 359–366.

[13] Lizarraga-Garcia, E., Buongiorno, J., Al-Safran, E., Lakehal, D., (2017) A broadly-applicable unified closure relation for Taylor bubble rise velocity in pipes with stagnant liquid. International Journal of Multiphase Flow 89, 345–358.

[14] Livinus, A., Verdin, P., Lao, L., Nossen, J., Langsholt, M., Sleipnæs, H., (2018) Simplified generalised drift velocity correlation for elongated bubbles in liquid in pipes. Journal of Petroleum Science and Engineering 160 106–118.

[15] Tang, H., Baily, W. J., and Killough, J. (2019) A Unified Gas/Liquid Drift-Flux Model for All Wellbore Inclinations. SPE Journal. DOI: 10.2118/197068-PA.

[16] Bhagwat, S. M. and Ghajar, A. J. (2014) A Flow Pattern Independent Drift Flux Model Based Void Fraction Correlation for a Wide Range of Gas-Liquid Two Phase Flow. Int. J. Multiphase Flow 59 (February): 186–205.

[17] Zuber, N., Findlay, J., (1965) Average volume concentration in two phase systems. ASME J. Heat Transf. 87, 453–468.

[18] Franca, H., Lahey, R.T., (1992) The use of drift flux techniques for the analysis of horizontal two phase flows. Int. J. Multiph. Flow 18, 787–801.

[19] Danielson, T.J., Fan, Y., (2009) Relationship between mixture and two-fluid models. In: Proceedings of the BHR Group International Conference on Multiphase Production Technology, June 17–19, Cannes, France.

[20] Choi, J., Pereyra, E., Sarica, C., Park, C., Kang, J.M., (2012) An efficient drift flux closure relationship to estimate liquid holdups of gas–liquid two phase flow in pipes. Energies 5, 5294–5306.

[21] Choi, J., Pereyra, E., Sarica, C., Lee, H., Jang, I.S., Kang, J.M., (2013) Development of a fast transient simulator for gas–liquid two-phase flow in pipes. Journal of Petroleum Science and Engineering 102, 27–35.

[22] Gokcal, B., (2005) Effects of High Viscosity on Two-Phase Oil–Gas Flow Behaviour in Horizontal Pipes. M.S. Thesis. University of Tulsa, Tulsa, OK, USA.

[23] Ben-Mansour, R., Al-Sarkhi, A., Sharma, A. K. et al. (2010) Effect of Pipe Diameter and High Oil Viscosity on Drift Velocity for Horizontal Pipes. Presented at the 7th North American Conference on Multiphase Technology, Banff, Canada, 2–4 June. BHR-2010-F3.

[24] Livinus, A., (2018) A study of a single elongated bubble in liquid in pipes. PhD Thesis, Cranfield University, Cranfield, UK.

[25] Livinus, A., and Verdin, P.G., (2020) Experimental study of a single elongated bubble in liquid in under 10-degree upwardly inclined pipes, Experimental Thermal and Fluid Science (2020), doi: https://doi.org/10.1016/j.expthermflusci.2020.110247

[26] Brunton, S.L., Noack, B.R., Koumoutsakos, P., (2020) Machine learning for fluid mechanics. Annual Review of Fluid Mechanics 52, 477 - 508.

[27] Amini, S. and Mohaghegh, S. (2019) Application of machine learning and artificial intelligence in proxy modelling for fluid flow in porous media. Fluids, 4,126; doi:10.3390/fluids4030126

[28] Nathaniel, S.E. and Livinus, A., (2022) Artificial Neural Network approach to the prediction of drift velocity of elongated bubble in liquid in pipe. SPE paper SPE-211941-MS, presented at NAICE, Lagos, Nigeria, August 2022.

[29] Koffi, I.U. and Livinus, A., (2022) Prediction of drift velocity closure relationship in multiphase flow models using deep learning approach. SPE paper SPE-211926-MS, presented at NAICE, Lagos, Nigeria, August 2022.

[30] Elkatatny, S. and Mahmoud, M., (2018) Development of new correlations for the oil formation volume factor in oil reservoirs using Artificial Intelligent White Box Technique. Petroleum. 4(2), pp. 178-186. https://doi.org/10.1016/j.petlm.2017.09.009. Pp 178-186

[31] Wallis, G.B., (1969) One-dimensional two-phase flow, McGraw-Hill, New York.

[32] Tung, K.W and Parlang, J.Y., (1976) Note on the motion of long bubbles in closed tubes - Influence of surface tension. Acta Mechanica 24, 313-317.

[33] Weber, M.E., (1981) Drift in intermittent two-phase flow in horizontal pipes. The Canadian Journal of Chemical Engineering. 59(3), 398–399.

[34] Pablo Valdés, J., Pico, P., Pereyra, E., Ratkovich, N. (2020) Evaluation of drift-velocity closure relationships for highly viscous liquid-air slug flow in horizontal pipes through 3D CFD modelling, Chemical Engineering Science DOI: https://doi.org/10.1016/j.ces.2020.115537.

[35] Bendiksen, K.H., (1984) An Experimental Investigation of the Motion of Long Bubbles in Inclined Tubes. International Journal of Multiphase Flow. 10(4), 467–483.

[36] Dumitrescu, D.T., (1943) Strömung an einerLuftblaseimsenkrechten Rohr. ZAMM - Zeitschrift für AngewandteMathematik und Mechanik. 23(3), 139–149. Available at: 10.1002/zamm.19430230303 (Accessed: 7 August 2015).

[37] Davies, R.M. and Taylor, G., (1950) The Mechanics of Large Bubbles Rising through Extended Liquids and through Liquids in Tubes. Proceedings of the Royal Society A: Mathematical, Physical and Engineering Sciences, 200(1062), 375–390. Available at: 10.1098/rspa.1950.0023.

[38] Benjamin, T.B., (1968) Gravity currents and related phenomena. Journal of Fluid Mechanics. 31(02), 209–248.

[39] Brown, R.A.S, (1965) The mechanics of large bubbles in miniaturized circular and noncircular channels. International Journal of Multiphase Flow. 27, 561-570.

[40] Hasan, a. and Kabir, C., (1988) Predicting Multiphase Flow Behavior in a Deviated Well. SPE Production Engineering. 3(4)

APPENDIX

The Froude number,Fr, is the ratio of the bubble inertia to the gravitational forces;

$$Fr = v_d/[(gD)(1 - {}^{\rho_g}/_{\rho_l})]^{1/2} \quad \text{(A-1)}$$

The Eötvös number, Eo, represents the ratio of the gravitational forces to the interfacial forces;

$$Eo = \frac{(\rho_l - \rho_g)gD^2}{\sigma} \quad \text{(A-2)}$$

The buoyancy Reynolds number,R, is the ratio of the gravitational forces to the viscous forces;

$$R = \frac{\left(D^3 g\left(\rho_l - \rho_g\right)\rho_l\right)^{0.5}}{\mu_l} \quad \text{(A-3)}$$

TableA-1. *Summary of some drift velocity correlations in liquid in pipes*

Authors	Correlation/model	Applicability Range	Equation No.
Dumitrescu [36]	$v_d^v = 0.351\sqrt{gD}$	90°, 1cP	(A-4)
Davies and Taylor [37]	$v_d^v = 0.328\sqrt{gD}$	90°, 1cP	(A-5)
Benjamin [38]	$v_d^h = 0.542\sqrt{gD}$	0°, 1cP	(A-6)
Brown [39]	$v_d^v = 0.35\sqrt{gD}\sqrt{1 - 2\left(\frac{\sqrt{1 + \mathrm{N}\,D} - 1}{\mathrm{N}\,D}\right)}$ The applicability limits of the above equation were	90°	(A-6a)

	reported as:		
	$$N = \left(14.5\frac{\rho_l^2 g}{\mu^2}\right)^{1/3}$$		(A-6b)
	Surface tension: $\frac{\rho_l g D^2}{4\sigma}\left(1-2\left(\frac{\sqrt{1+N_D}-1}{N_D}\right)\right)^2 > 5.0$		(A-6c)
	Viscosity: N D> 60.		(A-6d)
Wallis [31]	$$v_d^v = k\left[\frac{Dg(\rho_l-\rho_g)}{\rho_l}\right]^{0.5}$$ where	90°	(A-7a)
	$$k = 0.345\left(1-e^{-0.01R/0.345}\right)\left(1-e^{(3.37-Eo)/m}\right)$$		(A-7b)
	$$R = \frac{\left[D^3 g(\rho_l-\rho_g)\rho_l\right]^{0.5}}{\mu}$$		(A-7c)
	$$\begin{cases} m = 10, & R > 250 \\ m = 69R^{-0.35} & 18 < R < 250 \\ m = 25 & R < 18 \end{cases}$$		(A-7d)
Tung and Parlange[32]	$$Fr = \frac{v_d^v}{\sqrt{gD}} = \left(0.136 - 0.944\frac{\sigma}{\rho g D^2}\right)^{0.5}$$	90°	(A-8)
Weber [33]	$$\frac{v_d^h}{\sqrt{gD}} = 0.54 - 1.76Eo^{-0.56}$$ where	0°	(A-9a)
	$$Eo = \rho D^2 g/\sigma$$		(A-9b)
Bendiksen [35]	$$v_d = v_d^h cos\theta + v_d^v sin\theta$$ where	0° – 90°, 1cP	(A-10a)
	$$v_d^h = 0.542\sqrt{gD}$$		(A-10b)
	$$v_d^v = 0.351\sqrt{gD}$$		(A-10c)
Weber et al. [7]	$$v_d = v_d^h cos\theta + v_d^v sin\theta + 1.37(\Delta v_d)^{2/3} sin(\theta)(1 - sin(\theta))$$ when	0° – 90°	(A-11a)
	$$\Delta v_d = v_d^v - v_d^h > 0$$		(A-11b)
	$v_d = v_d^h cos\theta + v_d^v sin\theta$, when $\Delta v_d \le 0$		(A-11c)
Hasan and Kabir [40]	$$v_d = v_d^v\sqrt{sin\theta}(1+cos\theta)^{1.2}$$	30°– 90°, 1cP	(A-12a)
	$$v_d^v = 0.351\sqrt{gD}$$		(A-12b)
Gokcal et al. [10]	$$v_d = v_d^v(sin\theta)^{0.7} + v_d^h(cos\theta)^{1.5}$$ where	0° – 90°	(A-13a)
	$$v_d^v = -\frac{4}{3}\frac{\mu}{\rho.r} + \sqrt{\frac{4}{9}gr + \frac{16}{9}\frac{\mu^2}{(\rho.r)^2}}$$		(A-13b)
	$$v_d^h = V_2(1-\beta)$$		(A-13c)

	$\beta = \frac{\gamma - 0.5\sin 2\gamma}{3.142}$		(A-13d)
	$V_2 = \sqrt{2g[r(1-cos\gamma) - \Delta]}$		(A-13e)
	$\Delta = \frac{1-\beta}{\beta}\left(r(1-\cos\gamma) - \left[\frac{r[1-(1-\beta)cos\gamma] + 0.2122sin\gamma}{1-\beta^2}\right]\right) 2.2$		(A-13f)
Jeyachandra et al. [11]	$Fr_\theta = Fr^h cos\theta + Fr^v sin\theta$	0°– 90°	(A-14a)
	$Fr^h = 0.53e^{-13.7N_\mu^{0.46}E_o^{-0.1}}$		(A-14b)
	$Fr^v = -\frac{8}{3}N_{vis} + \sqrt{\frac{2}{9}\frac{\rho_L}{\rho_L - \rho_G} + \frac{64}{9}N_{vis}^2}$		(A-14c)
	$N_{vis} = \mu\left(gD^3(\rho_l - \rho_g)\rho_l\right)^{-0.5}$		(A-14d)
Choi et al. [20, 21]	$v_d = 0.0246cos(\theta) + 1.606\left(\frac{g\sigma\Delta\rho}{{\rho_L}^2}\right)^{1/4}\sin(\theta)$	0° – 90°	(A-15)
Moreiras et al. [12]	$Fr_H = 0.54 - \frac{N_{vis}}{1.886 + 0.01443N_{vis}}$	0° – 90°, $D \geq$ 0.0373m	(A-16a)
	$Fr_V = -\frac{8}{3}N_{vis} + \sqrt{\frac{2}{9}\frac{\rho_L}{\rho_L - \rho_G} + \frac{64}{9}N_{vis}^2} - \left(\frac{\sqrt{2}}{3} - 0.35\right)\sqrt{\frac{\rho_L}{\rho_L - \rho_G}}$		(A-16b)
	$Fr = Fr_H cos(\theta)^{1.2391} + Fr_V sin(\theta)^{1.2315} + Q$		(A-16c)
	$Q = 0, \text{if} Fr_V - Fr_H < 0$		(A-16d)
	Otherwise $Q = 2.1589(Fr_V - Fr_H)^{0.70412}sin\theta(1 - sin\theta)$		(A-16e)
Livinus et al. [14]	$Fr_l = 10^{-m}$	0° – 90°, μ_l< 7120cP	(A-17a)
	$m = 7.928E-07\left(-log_{10}\frac{R}{Eo}\right)^{7.443} + 0.3276$		(A-17b)
	$Fr_l^\theta = Fr_l(cos\theta + sin\theta)$		(A-17c)
Pablo Valdés et al. [34]	$Fr_H = 0.76419 - \frac{N_{vis}}{0.02418 + 2.15042N_{vis}} - (0.28879exp(Eo^{-0.50932}))$	0°	(A-18)

Citation: *Aniefiok Livinus. (2023). "Closing Thoughts on the Proposition of Improving Drift Velocity Closure Relationship for Multiphase Flow Models", International Journal of Petroleum and Petrochemical Engineering (IJPPE), 8(1), pp.18-35, DOI: http://dx.doi.org/10.20431/2454-7980.0801003*